

Hydrogel scaffolds with elasticity-mimicking embryonic substrates promote cardiac cellular network formation

Matthew Alonzo^{1,2}, Shweta Anil Kumar^{1,2} (0000-0001-9170-1686), Shane Allen⁴, Monica Delgado^{1,2} (0000-0003-2971-6849), Fabian Alvarez-Primo^{1,2} (0000-0002-6917-723X), Laura Suggs⁴, Binata Joddar^{1,2,3*} (0000-0002-9157-3140)

¹Inspired Materials & Stem-Cell Based Tissue Engineering Laboratory (IMSTEL),

²Department of Metallurgical, Materials and Biomedical Engineering, M201 Engineering, University of Texas at El Paso, 500 W University Avenue, El Paso, TX 79968, USA.

³Border Biomedical Research Center, University of Texas at El Paso, 500 W University Avenue, El Paso, TX 79968, USA

⁴Department of Biomedical Engineering, The University of Texas at Austin, 1 University Station, Austin, TX 78712, USA.

*Corresponding Author: bjoddar@utep.edu.

KEYWORDS: alginate, cardiomyocytes, elastic modulus, cell viability, scaffold stiffness

ABSTRACT

Stiffness of the extracellular matrix (ECM) in 3D-hydrogels that represent microcellular environments, influence cell phenotype, morphology and behavior. However, the composition of the ECM is highly dynamic, leading to alterations in matrix stiffness during developmental, normal and diseased physiology. To understand the role of the ECM in modulation of cardiac cell function during these various physiological states, we developed a system in which a mixture of alginate, calcium carbonate and D-glucono-delta-lacton (GDL) was used to yield gels with stiffness' mimicking embryonic-, physiologic- and fibrotic-states respectively. This system was employed to investigate the regulation of cardiomyocyte behavior. While the cardiomyocytes cultured within soft embryonic gels demonstrated cell spreading, elongation and network formation, progressive increase in gel stiffness diminished these behaviors while maintaining cell viability in all samples. Modulation of scaffold stiffness may pose as a valuable tool for modelling of cell behavior in biophysiological processes such as in cardiac fibrosis and other disease pathology.

Introduction

Tissue stiffness is a dynamic biomechanical property that influences organismal development and physiology (Chen and Liu 2016; Stowers et al. 2015). As the extracellular matrix (ECM) undergoes remodeling during various biological processes, the mechanical properties of the environment in which living cells are embedded changes accordingly. It is well established that variances in substrate stiffness can affect cellular migration, alignment, proliferation, morphology, and differentiation (Lee and Mooney 2001; Yang et al. 2017). In the human heart, the elastic modulus of the myocardium develops from an embryonic value in the low kPa regime (2-4 kPa) (Engler et al. 2008) to its mature physiologic value of about 9-12 kPa (Jacot et al. 2008). The elasticity of cardiac tissue can significantly increase beyond these values after cardiac fibrosis resulting from hypertrophy or myocardial infarction (Pandey et al. 2018).

Moreover, the biophysical characterization of the extracellular environment of cardiomyocytes has been shown to disrupt calcium transients, force generation, and alignment of sarcomeres during maturation (Jacot et al. 2008). However, a major challenge in the field is unravelling mechanotransduction pathways or the molecular mechanisms by which cells sense and respond to mechanical signals. Hydrogels are a class of biomaterials that are used to mimic the three-dimensional -ECM found in native cardiac tissues because they are biocompatible, biodegradable, and provide mechanical support to developing tissue. Additionally, they are highly porous, enabling cells to migrate and populate the scaffold and permitting the effective distribution of nutrients to be delivered to cells to meet their metabolic needs.

Various elastic hydrogels with ~99% aqueous media can be formulated at physiological conditions with maintenance of cell viability and function (Joddar et al. 2016; Lim and Sun 1980). Among these hydrogels, alginates have demonstrated extensive applicability as scaffolds for cell culture by ionically crosslinking in the presence of divalent Ca^{2+} ions (Lim and Sun 1980; Sun and Tan 2013). The widespread applicability of alginate hydrogels has been extended to culturing different cell types, both *in-vivo* and *in-vitro* (Andersen et al. 2015; Mondal et al. 2019). Alginate is a naturally derived hydrogel from seaweed. Its linear molecular backbone is composed of (1,4)-linked β -D-mannuronate (M) and α -L-guluronate (G) residues in varying contents and distributions along the length of the polymer (Kuen Yong Lee 2012; Petra Eiselt 2000). Although the proportion of M to G residues varies, alginate can be more readily crosslinked as more G residues are present in the molecule along with divalent cations such as Ca^{2+} . Some of the well-known benefits of alginate hydrogels are gelation at physiological conditions, which permit transparency for microscopic evaluation and enable retention of

homogenous, porous network formation that allows diffusion of nutrients and removal of waste (Drury and Mooney 2003).

Furthermore, cells can be extracted from these hydrogels using mild dissolution conditions that permit retention of all native cell behavior and morphology (Andersen et al. 2015). However, these alginate gels are mechanically insufficient, towards their use as scaffolds to engineer robust biological tissues such as cardiac tissue. In a previous study, we sought to address this challenge via encapsulation of multi-walled carbon nanotubes (MWCNT) serving as a reinforcing phase while being dispersed in a continuous phase of alginate (Joddar et al. 2016). Since the high doses of MWCNT were relatively cytotoxic, we next established an alternate method of dissolving CNT in surfactants for their homogenous dispersion, which also affords cytocompatibility (Alvarez-Primo et al. 2019). This and other such studies (Yildirim et al. 2008), create the need for well-characterized alginates with high purity and consistent mechanical properties for cell encapsulation.

In this study, we adopted an alginate-based hydrogel system (Stowers et al. 2015) that was used to create scaffolds with biomechanical properties depicting various developmental and disease states in cardiac tissues, namely, embryonic (soft), physiological (compliant/ normal) and fibrotic (stiff) states. Human cardiomyocytes were cultured in these three distinct gels, and the resulting differences in morphology, intercellular network formation, and characteristic protein expression profile were compared. We hypothesized that cardiomyocytes in stiffer scaffolds would express altered behavior, including reduced cell spreading, elongation, and network formation when compared to cells cultured in softer scaffolds.

Therefore, results from this study will reveal important information about the regulation of cardiomyocyte cell behavior in response to mechanical variances in the extracellular microenvironment. In summary, merely by modulating the surrounding scaffold stiffness, we expected to identify and reveal important physiological changes in the cultured cardiomyocytes, which may be recapitulative of cardiac disease or fibrosis *in-vivo*.

Materials and methods

Materials

MVG alginate (medium viscosity, high G content; Nova Matrix, Norway) was used to create three distinct gels of varying elastic moduli and was combined with Matrigel Matrix (Corning Inc., Corning, NY, USA) to provide points of cell adhesion within the crosslinked gels. According to the manufacturer, the alginate has greater than 60% G character. Calcium carbonate (CaCO_3 ; Fisher Scientific, Fair Lawn, NJ, USA) and D-(+)-

Gluconic acid δ -lactone (GDL; Millipore Sigma, St. Louis, MO) were used as crosslinking agents. A buffer solution was created with sodium chloride (NaCl; Fisher Scientific, Fair Lawn, NJ, USA) and 1 M HEPES buffer solution (Fisher Scientific, Fair Lawn, NJ, USA).

Gel formulation

Alginate gels of varying stiffness were created, as described in **Table 1**. In brief, Matrigel was mixed in a 25% volume of total gel, with an alginate solution (40% of the total gel volume) and vortexed to ensure homogeneity. All solutions were sterile filtered, with the exception of the alginate solutions, which were autoclaved. Half of the total prescribed buffer solution (20% of the total gel volume; 300 mM NaCl + 1 mM HEPES) was then added to the alginate mixture and vortexed once again to further dissolve any unmixed powder. Meanwhile, the other half of the buffer was mixed separately with calcium carbonate (5% of the total gel volume) and GDL (5% of the total gel volume) to create a dilute crosslinking solution. After seeding cardiomyocytes into the 24-well plate with the alginate (cell culture), the crosslinking solution is then pipetted into the well and mixed to ensure cell encapsulation by the crosslinked alginate gel. For the cell assays, the cell mixture represented 5% of the total gel volume and all other solutions were sterile filtered using 0.2 μ m filters (Aerodisc LC 25 mm, PALL Life Sciences, Ann Arbor, MI, USA) prior to the gel preparation. Gels used for characterization, were crosslinked without the addition of cells, which consisted of 25% buffer solution. Similarly, gels made without Matrigel but with cells consisted of 45% buffer solution.

Table 1. Concentrations of alginate, calcium carbonate, and GDL are shown for embryonic, physiologic, and fibrotic gels (from left to right).

Gel Type	Alginate (40% of total volume)	Calcium Carbonate (5% of total volume)	GDL (5% of total volume)
<i>Embryonic</i>	4% MVG	17.45 mg/ml or 0.17 mM	62.1 mg/ml or 0.35 mM
<i>Physiologic</i>	7% MVG	45.35 mg/ml or 0.45 mM	161.4 mg/ml or 0.91 mM
<i>Fibrotic</i>	10% MVG	50 mg/ml or 0.5 mM	177.9 mg/ml or 1 mM

Rheology

The mechanical stiffness of alginate gels was analyzed by conducting measurements on an Anton-Paar MCR 101 rheometer (Anton-Paar, Graz, Austria) with an 8 mm parallel plate configuration that performed oscillatory shear stress sweeps of 1% strain at frequencies from 0.5 to 50 Hz. The values for modulus were taken at 1.99 Hz for all groups, and the elastic modulus was determined via the storage and loss moduli obtained for all samples, using the formula (1):

$$E = (1 + v) \times G \quad \text{--- (1)}$$

In the above formula, G is the modulus of rigidity or shear modulus, E is the elastic modulus, and v is the Poisson's ratio (Stowers et al. 2015). Prior to rheometric analysis, gel samples were processed by cutting a cylindrical punch of about 8 mm in diameter and 1 mm in thickness. The cylindrical cut-outs were allowed to swell in 1X PBS for twelve hours before rheological testing.

Scanning Electron Microscopy (SEM) Imaging and Analysis of ultrastructure

Cross-sectional images of the lyophilized gel discs were collected using SEM, following published procedures (Alvarez-Primo et al. 2019). For SEM imaging, uniform-sized gel discs were lyophilized and sputter-coated with gold/palladium (2–3 min) in a sputter coater (Gatan Model 682 Precision etching coating system, Pleasantown, CA, USA) and visualized using SEM (S-4800, Hitachi, Japan) at voltages of 12-15 kV at varying magnifications. Collected images obtained were analyzed using Image J (NIH) to determine their average pore diameter (μm) and how the variation in stiffness across the samples affected this parameter.

Swelling Analysis

To account for the hydration and the swelling behavior of the gel scaffolds, samples were allowed to swell to equilibrium for up to 8 hr in Dulbecco Modified Eagle's Medium (DMEM, pH = 7, 25°C) following published protocols (AnilKumar et al. 2018). All gels samples were crosslinked and stored at -80°C (12 hr) following which they were freeze-dried using a VirTis BenchTop Pro Freeze Dryer with Omnitronics (SP Scientific, Warminster, PA, USA). These dried samples were weighed (W_0) and then immersed in DMEM, and the increase in weight was recorded periodically (W_t) at every 1 hr interval for the total duration of this experiment. The swelling ratio was calculated using the following equation (2), where D_s was the degree of swelling, W_0 , and W_t were the weights of the samples in the dry and swollen states, respectively.

$$Ds = (W_t - W_0) / W_0 \quad \text{--- (2)}$$

Cell Culture in 3D gels

AC16 human cardiomyocyte cell line (CM, Millipore cat no. SCC109) were cultured in Dulbecco's Modified Eagle's Medium/Nutrient Mixture F-12 Ham (DMEM/F-12) supplemented with 10% fetal bovine serum (FBS) and 1% penicillin-streptomycin as reported previously and henceforth referred to as complete growth medium (Anil Kumar et al. 2019). Originally, this cell line was derived from the fusion of primary adult human ventricular heart tissue cells with SV40 transformed, uridine auxotroph human fibroblasts, lacking mitochondrial DNA (Davidson et al. 2005). Following the use of a uridine-free medium as a selection for the removal of unfused fibroblasts, the remaining fused cells were subcloned and screened for the presence of SV40 large T-ag, β -myosin heavy chain (β MHC) and connexin-43 (Cx 43) (Davidson et al. 2005). Therefore, these cells are similar in their physiological behavior to most human primary cardiomyocytes. Media was changed every 2 days, and cells were passaged before reaching confluence. To confirm the viability of cells post encapsulation in gels after crosslinking, the CM were labeled with PKH26 red fluorescent membrane staining dye (Sigma), as done before (Anil Kumar et al. 2019). For cell encapsulation studies, pre-stained cells were mixed with the alginate solution (1×10^6 cells/ml) before gelation to ensure a uniform distribution throughout the gels and crosslinked following procedure reported earlier. Alginate is not known to possess cell adhesive moieties; therefore, cell adhesion sites were introduced by the mixing of alginate solution with Matrigel (Stowers et al. 2015). These cell-gel constructs were cultured for 4- and 7-days (with complete growth medium, 37°C, 5% CO₂), respectively after, which these samples were imaged without fixing the cells in the gel-samples using confocal fluorescence microscopy (Zeiss). Gelatin (0.1%, Gibco, Invitrogen, Carlsbad, CA) and Matrigel (Corning) coated wells were used as controls for this experiment. For the controls, 1×10^5 cells/ well were seeded in 24 well-plates. At Day-4 and Day-7 images were acquired from the cells cultured within gels and aspect ratio calculations were performed using an equation (3) developed previously (Stowers et al. 2015).

Aspect ratio (unitless) = $\frac{\text{width}}{\text{height}}$ of a single cell ----- (3)

Cell Viability Assay

All samples with cells were examined using a Live/Dead assay (Thermo Fisher Scientific, Waltham, USA) with Calcein AM that stained the live cells green, and Ethidium homodimer that stained the dead cells red, respectively. After 5 days of culture, the cell-laden constructs were subjected to the Live/Dead assay. All Live/Dead stained cells were then imaged using a Zeiss Axiovert Inverted Phase Contrast Fluorescent Microscope, to confirm the retention of viable cells within the gel scaffolds and in non-gel controls. All images collected were

analyzed using quantitative image analysis through Image J. The percentage of live or dead cells was obtained based on equation (4) as follows:

$$\frac{\text{No. of live cells}}{\text{No. of dead cells}} (\%) = \frac{\text{No. of particles in green or red threshold image} * 100}{\text{Total no. of particles in green and red threshold images}} \quad \text{---(4)}$$

Cardiac Cx-43 and Troponin Protein Analysis

To understand how the gel stiffness modulates CM performance, AC16 cells were mixed in gels within 12-well plates, for a total of 48-hour culture period and cultured in complete growth media. Following completion of experimental period for culture, protein extraction procedures followed by analysis occurred as described below. Cell-gel samples were taken out carefully from the wells rinsed in 1X phosphate buffered saline (PBS) and cells extracted from the gels using 0.25% Trypsin-EDTA via addition of 110 µl of protease and phosphatase inhibitors, using procedures described earlier (Anil Kumar et al. 2019). The isolated AC16 cells were then sonicated and centrifuged to maximize protein quantification. Protein concentration was estimated on the Nanodrop for each sample, aliquot into individual tubes with a total of 25 µg of protein per tube. A total of 8 samples were then loaded onto a 10-well 12.5% polyacrylamide gel (Bio-Rad Mini Protean TGX stain-free) for separation of proteins and their subsequent analysis via western blotting. Primary antibodies were used to probe and detect cardiac Troponin I (cTnI) and Connexin-43 (Cx-43) while the housekeeping gene β-actin and GAPDH served as controls (mouse monoclonal primary antibody, 1:200, Millipore-Sigma), respectively. The blots were imaged and analyzed using SysStat application.

Statistical Analysis

All sets of experiments applied n=3 set of trials unless otherwise specified. Data is presented as the mean ± standard deviation. Statistical analysis was performed in each group using a one-way ANOVA and Tukey's multiple comparison test. *p<0.05 or lesser was deemed statistically significant.

Results and discussion

Following the exposure to Ca²⁺ ions, alginate reacts immediately, resulting in non-homogenous cross-linking and gel formation. To delay this instantaneous crosslinking, we adopted a sustained gelling mechanism that acts by the introduction of Ca²⁺ ions directly into the alginate matrix (Schmitt et al. 2015). Thus, homogeneously crosslinked alginate gels were made using insoluble CaCO₃ providing a source of calcium, and GDL, that is known to hydrolyze upon dissolution in water to release calcium ions, following published guidelines

from another study (**Fig. 1**) (Stowers et al. 2015). When the GDL is slowly hydrolyzed, it results in a drop in the pH of the solution and, subsequently, a release of Ca^{2+} ions from the CaCO_3 into the solution. We allowed a time-delayed release of calcium ions, resulting in the formation of homogenous alginate gels within one hour. Alginate gel formulation was optimized to yield characteristic stiffness's by testing 4-10 % (w/v) MVG alginate solutions against 10-50 mg/mL CaCO_3 (0.17-0.5 mM) solutions. It is well known that stiffness or elastic modulus of chemically crosslinked polymers is known to proportionately rise with increasing content of the basic monomer and the density of the crosslinking ions (Liu and Huglin 1995). After initial testing and rheological analysis of the crosslinked gels (**Supplementary Figure 1**), three formulations were selected to represent 'embryonic', 'physiologic', and 'fibrotic' respectively, which are referenced in **Table 1**.

It was found that these relevant stiffnesses can be achieved using this type of alginate polymer, especially due to the high guluronate content that makes the gels more readily crosslinkable. However, the molar concentration of GDL was always 3.5 times that of CaCO_3 to maintain a neutral pH. This range of concentration for CaCO_3 and GDL has been reported to be well tolerated by cells in other studies (Stowers et al. 2015). Not knowing how CM would specifically react to these gels and their crosslinking, we opted to work with extremely low concentrations of Ca^{2+} ions compared with published literature, which suggests the use of 50 mM CaCO_3 for crosslinking and gel formation to occur within 30 mins(Schmitt et al. 2015).

For cell encapsulation studies, cells were mixed with the alginate solution before gelation to ensure a uniform distribution throughout the gel. Optimized gels showed viscoelastic behavior, and the storage modulus was greater than the loss modulus for all hydrogel compositions. Furthermore, the average elastic moduli for the optimized embryonic, physiologic, and fibrotic gels were 2.66 ± 0.84 , 8.98 ± 1.29 , and 18.27 ± 3.17 kPa respectively (**Fig. 1A**), which were all significantly different from one another ($p<0.05$).

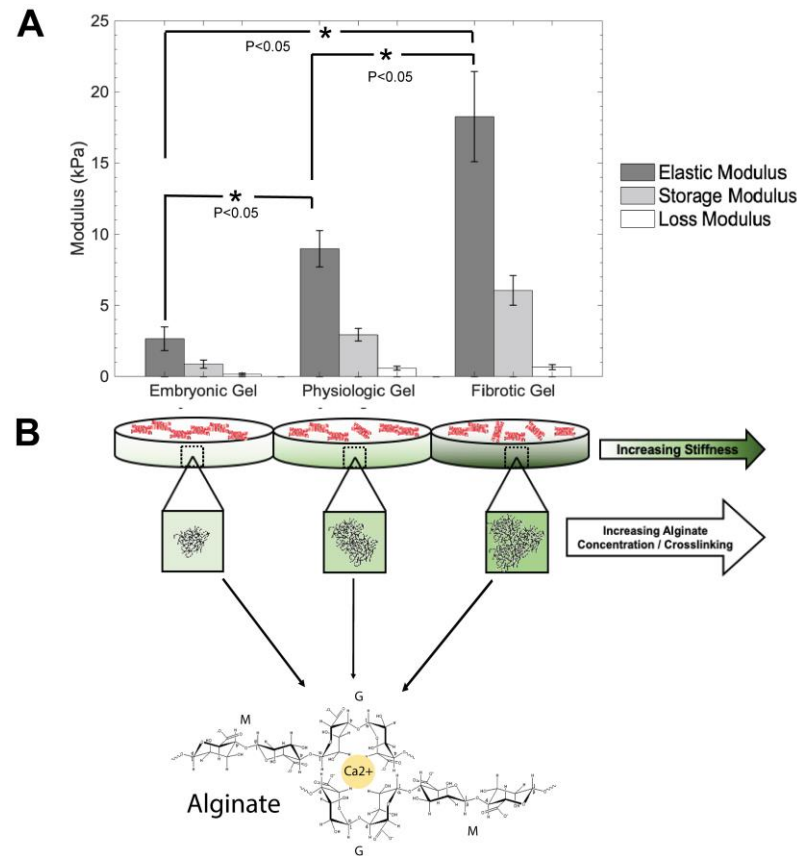


Fig. 1 Shown in **A** are the rheological properties of alginate gels, including Elastic-, Storage- and Loss-modulus.

In **B**, a schematic depicting the corresponding gels of increasing mechanical stiffness made by increasing the concentration of both the biopolymer and calcium crosslinking solution is included. p-values are all significant.

* 0.009; ** 0.008; *** 0.034

Analysis of electron micrographs revealed a highly porous interconnected architecture for all three gels permissive towards cell culture applications (Dewavrin et al. 2014), as can be seen by representative images in **Fig. 2A-C**. The average pore diameter (end-to-end length) was determined to be $51.2 \pm 2.8 \mu\text{m}$, $38.4 \pm 15.9 \mu\text{m}$, and $32.3 \pm 9.1 \mu\text{m}$ for the embryonic, physiologic, and fibrotic gels respectively as represented in Figure 2D and were all significantly different among the group. As shown by these results, the average pore diameter decreases with stiffness, which is also reported by another group (Annabi et al. 2010). Figure 2E depicts the swelling behavior of the embryonic, physiologic and fibrotic scaffolds in DMEM. The embryonic scaffolds were found to swell to a greater extent, whereas the fibrotic scaffolds appeared to swell the least. Since swelling behavior is dependent on the extent of polymer crosslinking (Khan and Ranjha 2014; Oh et al. 1998), these results could imply that the fibrotic scaffolds were crosslinked to a greater degree due to their increased alginate and CaCO_3 .

content, with respect to the physiological and embryonic scaffolds. However, the fibrotic scaffolds were observed to start deteriorating after the 48 hr mark. The embryonic scaffolds were relatively more stable and were noted to undergo further swelling. The physiologic scaffolds demonstrated the greatest stability in terms of reaching equilibrium and maintaining a stable swelling ratio without dissociating into smaller constituents. The swelling data were analyzed through a Two-Step Anova and corroborated with a Post-Hoc Honestly Significant Difference Tukey test, pointing towards a very highly significant difference in swelling ratio ($p<0.01$) observed in the embryonic tissue. Although the physiologic and fibrotic scaffolds posed almost no statistical difference between their swelling rates, their degradation was also noted in a similar manner, for which it was determined that the physiologic scaffolds maintained a higher integrity in comparison to the embryonic and fibrotic scaffolds, by maintaining a greater stability for longer periods of time, after reaching equilibrium in DMEM.

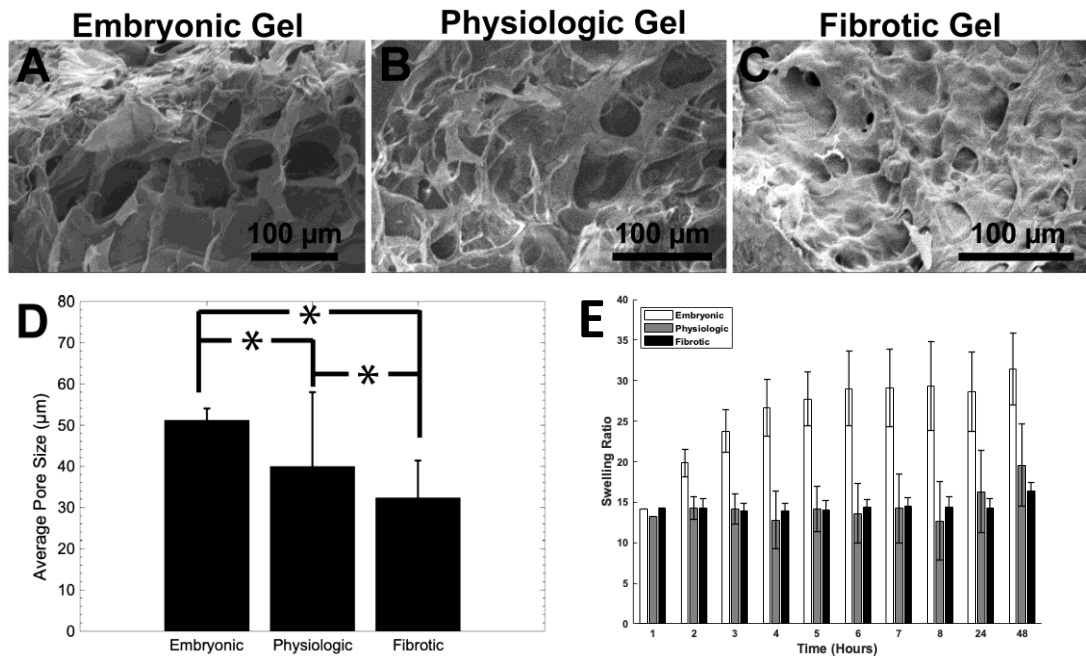


Fig. 2 Shown in A-C are representative SEM images captured to reveal their ultrastructure. **Panel D** shows the average pore size of each gel depicted in A-C. Panel E depicts the swelling behavior of the three different gels in DMEM

After 4- and 7-days, fluorescent images of cells forming networks within the gels were acquired. Shown in **Fig. 3A** are images acquired from samples at Day-4 (Top row) and at Day-7 of culture (Bottom row). From a comparison of both rows in **Fig. 3A**, cell proliferation in all three conditions was confirmed. However, in the entire alginate–Matrigel composite gels (**Fig. 3A**), we observed elongated cells in the embryonic gels that became more rounded with increased stiffening as was the case for cells in physiologic and fibrotic gels. This observation

was confirmed in **Fig. 3B**, where the average aspect ratio of cells in each gel sample is depicted. The aspect ratio for cells cultured in the embryonic gels was the highest, followed by the other two gels, respectively.

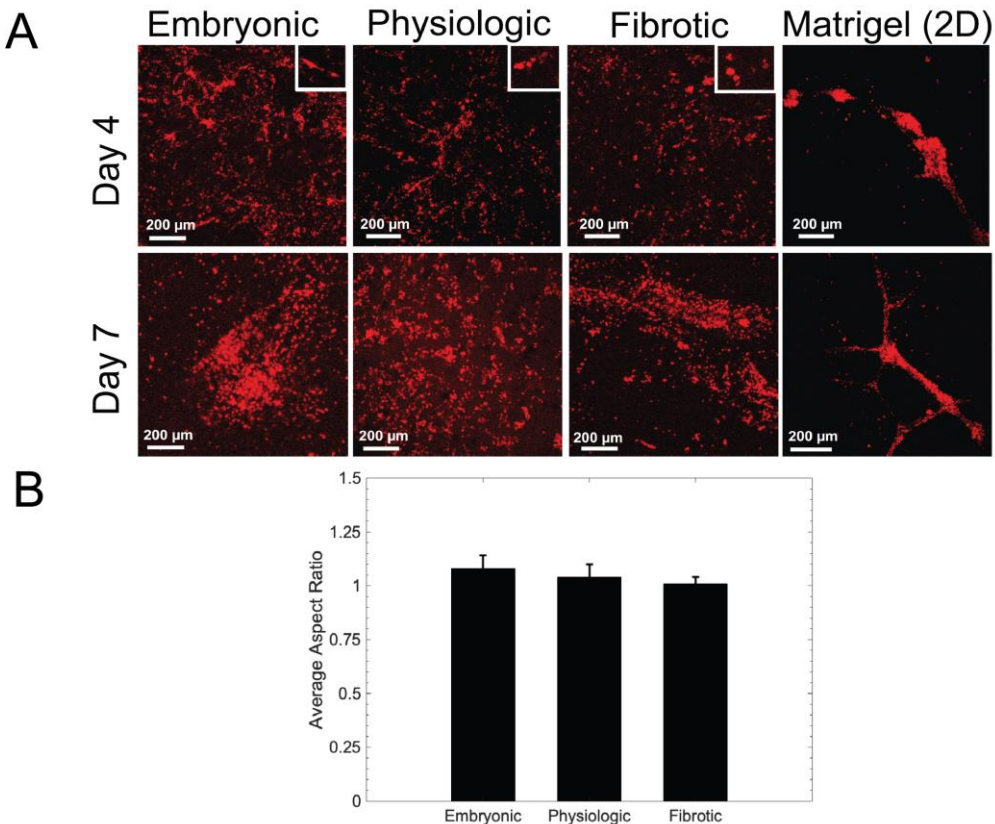


Fig. 3 Shown in **Panel A** are cells cultured within the 3D gels and on 2D Matrigel Controls. The cells were prestained with PKH26 (red) to reveal network formation in these cultures. Also, the magnified insets depict the elongated cell morphology within the embryonic gels, which become gradually rounded as the gels were progressively stiffened from the physiologic to the fibrotic gels. Shown in **Panel B** is the average cellular aspect ratio (width/height) for cells cultured within the gels. The aspect ratio is maximum in the case of cells cultured within the embryonic gels and is close to the value of 1 (implying rounded cells) as the gels were stiffened

Shown in **Fig. 4A** are brightfield images from all cell-gel samples acquired at Day-7, which clearly depict the network formation among proliferating cell cultures. For quantification purposes, a network was defined as a coupled pattern within a group of adjacent cells as established by others (Stowers et al. 2015). The average number of cellular networks per unit area of the sample imaged was calculated and represented in **Fig. 4B**. The embryonic gels contained a significantly higher number of networks, which proportionately decreased as the gel stiffness was increased. In embryonic gels, the cells were capable of enzymatic degradation or mechanical deformation of the matrix to form extensions into the gels. As the gels were progressively stiffened, the cells' ability to remodel

the matrix was diminished, and the cells appeared predominantly rounded, since the matrix was relatively stiffer to deform or because the degradation sites were obstructed by the introduction of additional crosslinks (Stowers et al. 2015). The cellular network behavior confirmation is provided by the representative image that clearly shows networks established by human AC16 cells when cultured atop Matrigel-coated 2D wells (**Supplementary Figure 2**). However, when Matrigel was excluded from the gels, no networks were evident after 5-days of culture even in the stiff gels, although the cells retained viability and depicted cluster formation (**Supplementary Figure 3**).

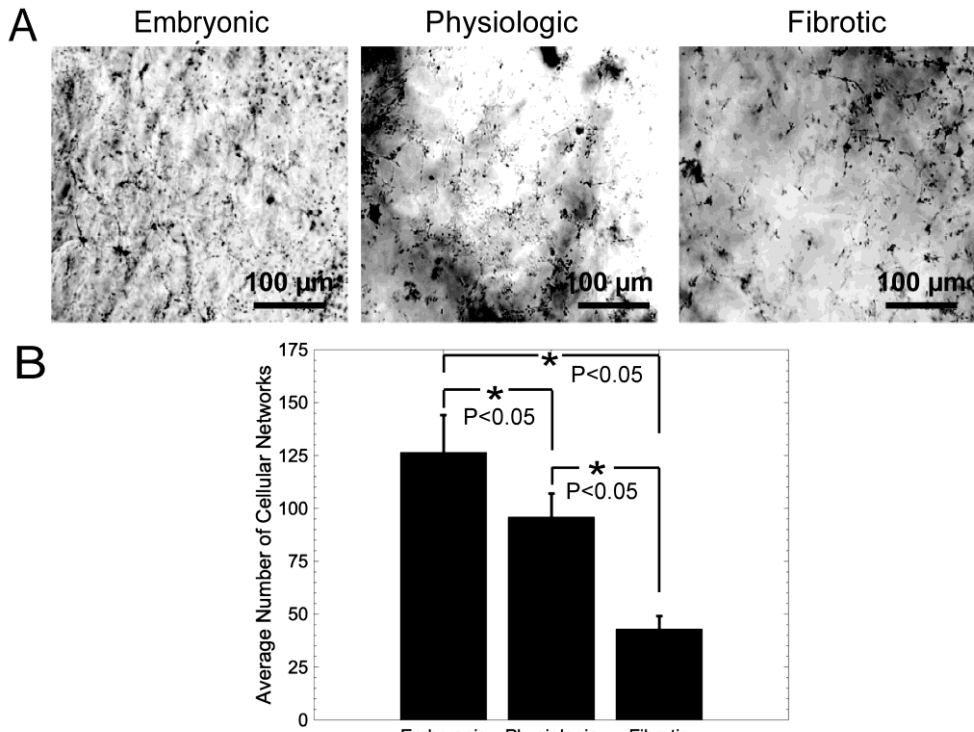
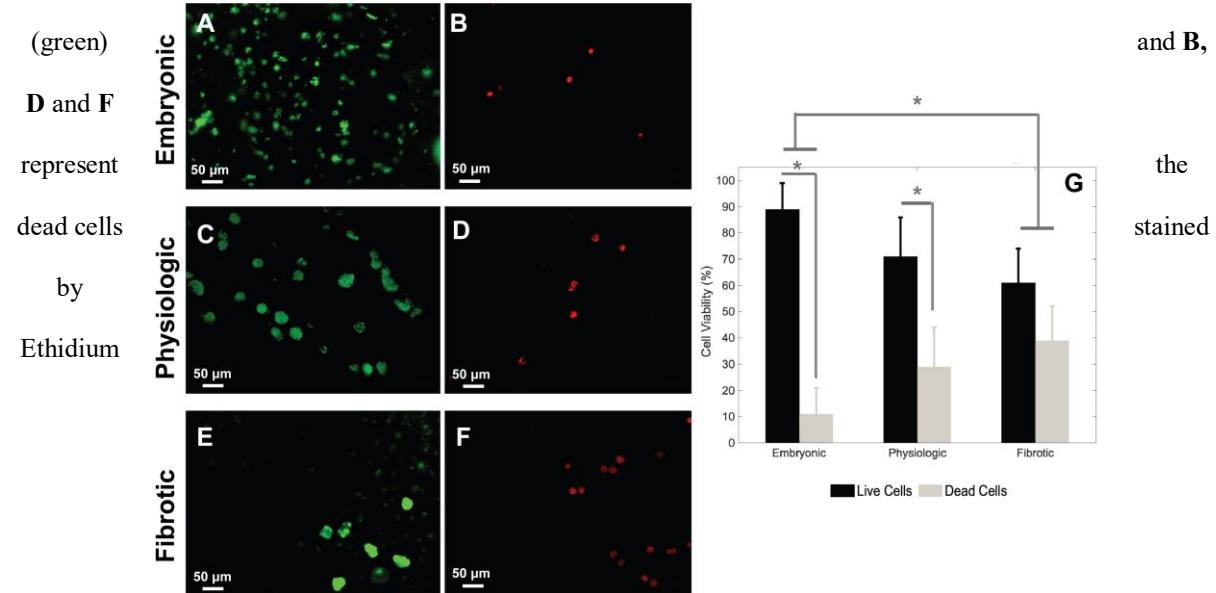


Fig. 4 Shown in **Panel A** are phase-contrast images of cellular networks cultured within the 3D gels and on 2D Matrigel Controls (**Supplementary Figure 2**). It is evident that the average number of cellular networks per unit area is significantly reduced as the gels were progressively stiffened. Shown in **Panel B** is the average number of cellular networks within all the gels. p-values are all significant

Cell viability determined with the Live/Dead assay revealed an increasing number of dead cells and a decreasing number of live cells as the stiffness of the alginate scaffold increased as seen in **Fig. 5**. Embryonic gels had $89 \pm 10\%$ live cells with $11 \pm 10\%$ dead cells, physiologic gels had $71 \pm 15\%$ live cells with $29 \pm 15\%$ dead cells, and fibrotic gels had $61 \pm 13\%$ live cells with $39 \pm 13\%$ dead cells within each scaffold respectively, as represented in **Fig. 5A-F**. There was a significant difference ($p < 0.05$) between the number of live to dead cells in both the embryonic and physiologic-mimicking scaffolds, however no such significance was seen in the fibrotic scaffold. Furthermore, there was a significant difference in the percentage of live and dead cells between the

embryonic and fibrotic scaffolds, as illustrated in **Fig. 5G**. The inverse trend in cell viability with respect to matrix stiffness can possibly be attributed to the diffusion barriers of nutrients and oxygen caused by the increased polymeric network associated with stiffer scaffolds as suggested by the decreased porosity results in **Fig. 2** and elucidated by others (Sawyer et al. 2016). Implications of this data can be extrapolated to explain why grafts in the zone of dense collagen deposition after myocardial infarction lead to reduced cell engraftment compared to softer grafts (Liang et al. 2019).

Fig. 5 Cell viability was assessed by performing the Live/Dead assay on cells within the embryonic, physiologic and fibrotic scaffolds after 5 days of culture. **A, C** and **E** depict the live cells stained by Calcein AM



homodimer (red) for the embryonic, physiologic and fibrotic scaffolds respectively. The number of live to dead cells in both the embryonic and physiologic scaffolds were found to be statistically significant ($p < 0.05$) unlike the fibrotic scaffolds. **G** depicts the percentage of live and dead cells for each of the three scaffolds. The live cell count was noted to decrease proportionately with increasing scaffold stiffness as has been validated by published works (Sawyer et al. 2016)

To further study the effects of scaffold stiffness on expression of cardiac-specific markers, Cx-43 and cTnI, cells were probed for these proteins using a Western blot (**Fig. 6**) in the softest and stiffest of the gels. Cx-43 is found at gap junction channels between neighboring cardiomyocytes. The protein plays a role in enhancing intercellular communication, electrical coupling, and promote synchronous contractility of the heart (You et al. 2011). The amount of Cx-43 was observed to be 1.5-times higher in softer gels and compared to stiffer ones (**Fig. 6A**), suggesting cardiomyogenesis is promoted in softer microenvironments leading to enhanced cellular communication and network formation as corroborated by the observed network formations seen in **Fig. 4**.

Amplification of Cx-43 in softer 3D substrates emphasizes hydrogel stiffness as an important factor for optimization of tissue-engineered cardiac constructs within hydrogels that are often used to mimic 3D environments of native tissues in-vitro (Anil Kumar et al. 2019; Li and Guan 2011).

Enhanced cTnI expression was observed in cells within fibrotic gels as compared to those cultured in soft embryonic gels by a factor of 1.3 as graphically illustrated in **Fig. 6B**. The cTnI protein is specific to cardiac tissue and commonly used as a marker for myocardial damage (Sharma et al. 2004). Other studies have also demonstrated cTnI is discharged from viable cardiomyocytes by stimulation of stretch-responsive integrins (Hessel et al. 2008). Thus, amplified cTnI in our system can be due to a combination of both factors. Cell viability

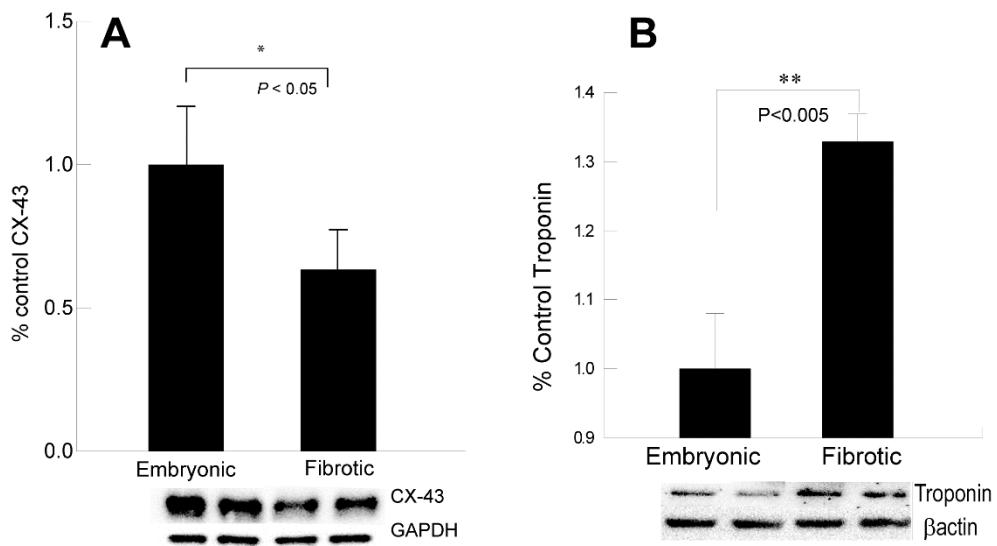


Fig. 6 Western blot analysis for cardiac biomarkers Cx-43 and Troponin are displayed between the softest (embryonic) and stiffest (fibrotic) gels in our study. Intercellular Connexin-43 (A) found in gap junctions between neighboring cardiomyocytes is expressed more in softer environments, while cTnI expression increases in stiffer gels (B).

is seen to decrease with increasing scaffold stiffness (Fig. 5) which could cause the upregulation of the cTnI stress biomarker due to the smaller pore size within the scaffold that would allow cell migration and gas exchange. Enhancement of cTnI can also be attributed to the high stretch-responsive mechanical stimulation of cellular integrins that interact with the stiff mechanical environment of the scaffold.

Conclusion

We have developed an alginate gel system that represents embryonic-, physiologic- and fibrotic-matrices by exhibiting the range of matrix stiffness that is common to these tissue states *in-vivo*. Our 3D system recapitulates the features of others reported works on 2D models reporting on the stiffness of the fetal, adult and fibrotic heart and their effects respectively (Pandey et al. 2018). Our system is cell compatible and is responsive to modeling dynamic phenomena, such as tissue fibrosis, to isolate the effects of matrix stiffening. We used this system to demonstrate the regulation of CM morphology by matrix stiffness in all gels. In summary, the soft embryonic gels permitted extensive cell spreading, elongation, and network formation. They further showed a greater expression of Cx-43 and reduced cTnI expression, On the contrary, the stiffer gels showed the progressively lesser extent of cell spreading, elongation, and network formation. The stiffest gel showed reduced Cx-43 and enhanced cTnI expression. In the future, we will explore the ability to dynamically control the gel stiffness, both spatially and temporally. Thus, it will be possible to translate *in-vitro* outcomes to more relevant *in-vivo* disease models while maintaining the hydrogel system composition constant.

Conflicts of Interest

There are no conflicts to declare.

Acknowledgements

The Joddar Lab (IMSTEL) acknowledges NIH 1SC2HL134642-01 and NSF (CBET 1927628). Matthew Alonso acknowledges the Eloise E. and Patrick B. Wieland fellowship at UTEP and the Gates Millennium Scholarship Program. Fabian Alvarez Primo acknowledges the Eloise E. and Patrick B. Wieland fellowship and the Dissertation Completion fellowship at UTEP. We acknowledge the technical assistance received from Dr. Armando Varela for kindly assisting us with the confocal microscopy. Research reported in this article was also supported by the National Institute of General Medical Sciences of the National Institutes of Health under Linked Award Numbers RL5GM118969, TL4GM118971, and UL1GM118970. The content is solely the responsibility of the authors and does not necessarily represent the official views of the National Institutes of Health. Authors also acknowledge support for Materials and supplies for this project obtained from NSF-PREM (DMR-1827745) and the NSF-MRI (DMR 1826268).

References

Alvarez-Primo F, Anil Kumar S, Manciu FS, Joddar B (2019) Fabrication of Surfactant-Dispersed HiPco Single-Walled Carbon Nanotube-Based Alginate Hydrogel Composites as Cellular Products. *International Journal of Molecular Sciences* 20:4802. <https://doi.org/10.3390/ijms20194802>

Andersen T, Auk-Emblem P, Dornish M (2015) 3D cell culture in alginate hydrogels. *Microarrays* 4:133-161. <https://doi.org/10.3390/microarrays4020133>

Anil Kumar S et al. (2019) A Visible Light-Cross-Linkable, Fibrin–Gelatin-Based Bioprinted Construct with Human Cardiomyocytes and Fibroblasts. *ACS Biomaterials Science & Engineering* 5:4551-4563 <https://doi.org/10.1021/acsbiomaterials.9b00505>

Anil Kumar S et al. (2018) The applicability of furfuryl-gelatin as a novel bioink for tissue engineering applications. *Journal of Biomedical Materials Research Part B: Applied Biomaterials*. <https://doi.org/10.1002/jbm.b.34123>

Annabi N, Mithieux SM, Weiss AS, Dehghani F (2010) Cross-linked open-pore elastic hydrogels based on tropoelastin, elastin and high pressure CO₂. *Biomaterials* 31:1655-1665. <https://doi.org/10.1016/j.biomaterials.2009.11.051>

Chen F-M, Liu X (2016) Advancing biomaterials of human origin for tissue engineering. *Progress in polymer science* 53:86-168. <https://doi.org/10.1016/j.progpolymsci.2015.02.004>

Davidson MM et al. (2005) Novel cell lines derived from adult human ventricular cardiomyocytes. *Journal of molecular and cellular cardiology* 39:133-147. <https://doi.org/10.1016/j.yjmcc.2005.03.003>

Dewavrin J-Y, Hamzavi N, Shim V, Raghunath M (2014) Tuning the architecture of three-dimensional collagen hydrogels by physiological macromolecular crowding. *Acta biomaterialia* 10:4351-4359. <https://doi.org/10.1016/j.actbio.2014.06.006>

Drury JL, Mooney DJ (2003) Hydrogels for tissue engineering: scaffold design variables and applications. *Biomaterials* 24:4337-4351. [https://doi.org/10.1016/S0142-9612\(03\)00340-5](https://doi.org/10.1016/S0142-9612(03)00340-5)

Engler AJ et al. (2008) Embryonic cardiomyocytes beat best on a matrix with heart-like elasticity: scar-like rigidity inhibits beating. *Journal of cell science* 121:3794-3802. <https://doi.org/10.1242/jcs.029678>

Hessel M, Atsma D, Van Der Valk E, Bax W, Schalij M, Van Der Laarse A (2008) Release of cardiac troponin I from viable cardiomyocytes is mediated by integrin stimulation. *Pflügers Archiv-European Journal of Physiology* 455:979-986. <https://doi.org/10.1007/s00424-007-0354-8>

Jacot JG, McCulloch AD, Omens JH (2008) Substrate Stiffness Affects the Functional Maturation of Neonatal Rat Ventricular Myocytes . Biophysical Journal 95:3479-3487. <https://doi.org/10.1529/biophysj.107.124545>

Joddar B, Garcia E, Casas A, Stewart CM (2016) Development of functionalized multi-walled carbon-nanotube based alginate hydrogels for enabling biomimetic technologies. Scientific reports 6. <https://doi.org/10.1038/srep32456>

Khan S, Ranjha NM (2014) Effect of degree of cross-linking on swelling and on drug release of low viscous chitosan/poly (vinyl alcohol) hydrogels. Polymer Bulletin 71:2133-2158. <https://doi.org/10.1007/s00289-014-1178-2>

Kuen Yong Lee DJM (2012) Alginate: Properties and Biomedical Applications. Progress in Polymer Science 37:106-126. <https://doi.org/10.1016/j.progpolymsci.2011.06.003>

Lee KY, Mooney DJ (2001) Hydrogels for tissue engineering. Chemical reviews 101:1869-1880. <https://doi.org/10.1021/cr000108x>

Li Z, Guan J (2011) Hydrogels for cardiac tissue engineering. Polymers 3:740-761. <https://doi.org/10.3390/polym3020740>

Liang J, Huang W, Jiang L, Paul C, Li X, Wang YJSC (2019) Concise Review: Reduction of Adverse Cardiac Scarring Facilitates Pluripotent Stem Cell-Based Therapy for Myocardial Infarction. Stem Cells 37:844-854. <https://doi.org/10.1002/stem.3009>

Lim F, Sun AM (1980) Microencapsulated islets as bioartificial endocrine pancreas. Science 210:908-910. <https://doi.org/10.1126/science.6776628>

Liu Y, Huglin MB (1995) Effective crosslinking densities and elastic moduli of some physically crosslinked hydrogels. Polymer 36:1715-1718 [https://doi.org/10.1016/0032-3861\(95\)99018-P](https://doi.org/10.1016/0032-3861(95)99018-P)

Mondal A et al. (2019) Characterization and printability of Sodium alginate-Gelatin hydrogel for bioprinting NSCLC co-culture. Scientific Reports 9:1-12. <https://doi.org/10.1038/s41598-019-55034-9>

Oh KS, Oh JS, Choi HS, Bae YC (1998) Effect of cross-linking density on swelling behavior of NIPA gel particles. Macromolecules 31:7328-7335. <https://doi.org/10.1021/ma971554y>

Pandey P et al. (2018) Cardiomyocytes sense matrix rigidity through a combination of muscle and non-muscle myosin contractions. Developmental Cell 44:326-336. e323. <https://doi.org/10.1016/j.devcel.2017.12.024>

Petra Eiselt JY, Rachel K. Latvala, Lonnie D. Shea, David J. Mooney (2000) Porous Carriers for Biomedical Applications Based on Alginate Hydrogels. *Biomaterials* 21:1921-1927. [https://doi.org/10.1016/S0142-9612\(00\)00033-8](https://doi.org/10.1016/S0142-9612(00)00033-8)

Sawyer S, Oest M, Margulies B, Soman P (2016) Behavior of encapsulated saos-2 cells within gelatin methacrylate hydrogels. *Journal of Tissue Science and Engineering* 7:2. <http://dx.doi.org/10.4172/2157-7552.1000173>

Schmitt A et al. (2015) Calcium alginate gels as stem cell matrix-making paracrine stem cell activity available for enhanced healing after surgery. *PLoS One* 10:e0118937-e0118937 doi:10.1371/journal.pone.0118937

Sharma S, Jackson P, Makan J (2004) Cardiac troponins. BMJ Publishing Group. <http://dx.doi.org/10.1136/jcp.2003.015420>

Stowers RS, Allen SC, Suggs LJ (2015) Dynamic phototuning of 3D hydrogel stiffness. *Proceedings of the National Academy of Sciences* 112:1953-1958. <https://doi.org/10.1073/pnas.1421897112>

Sun J, Tan H (2013) Alginate-based biomaterials for regenerative medicine applications *Materials* 6:1285-1309. <https://doi.org/10.3390/ma6041285>

Yang Y, Wang K, Gu X, Leong KW (2017) Biophysical regulation of cell behavior—cross talk between substrate stiffness and nanotopography *Engineering* 3:36-54. <https://doi.org/10.1016/J.ENG.2017.01.014>

Yildirim ED, Yin X, Nair K, Sun W (2008) Fabrication, characterization, and biocompatibility of single-walled carbon nanotube-reinforced alginate composite scaffolds manufactured using freeform fabrication technique. *Journal of Biomedical Materials Research Part B: Applied Biomaterials: An Official Journal of The Society for Biomaterials, The Japanese Society for Biomaterials, and The Australian Society for Biomaterials and the Korean Society for Biomaterials* 87:406-414. <https://doi.org/10.1002/jbm.b.31118>

You J-O, Rafat M, Ye GJ, Auguste DT (2011) Nanoengineering the heart: conductive scaffolds enhance connexin 43 expression. *Nano letters* 11:3643-3648. <https://doi.org/10.1021/nl201514a>

Hydrogel scaffolds with elasticity-mimicking embryonic substrates promote cardiac cellular network formation

Matthew Alonzo^{1,2}, Shweta Anil Kumar^{1,2} (0000-0001-9170-1686), Shane Allen⁴, Monica Delgado^{1,2} (0000-0003-2971-6849), Fabian Alvarez-Primo^{1,2} (0000-0002-6917-723X), Laura Suggs⁴, Binata Joddar^{1,2,3*} (0000-0002-9157-3140)

¹Inspired Materials & Stem-Cell Based Tissue Engineering Laboratory (IMSTEL),

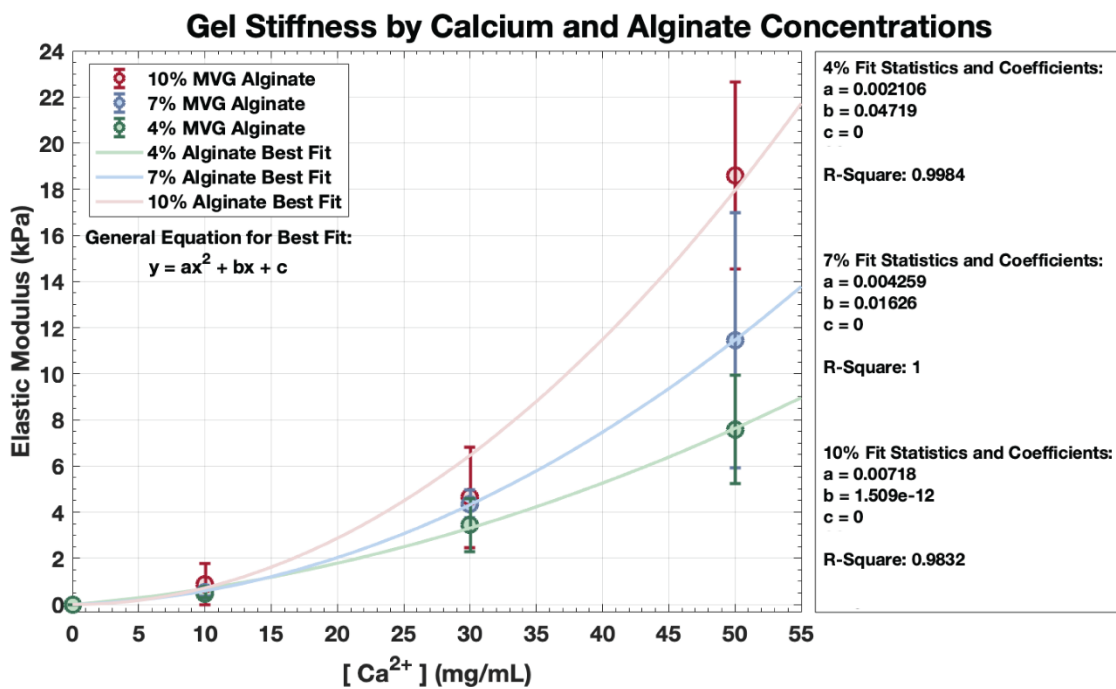
²Department of Metallurgical, Materials and Biomedical Engineering, M201 Engineering, University of Texas at El Paso, 500 W University Avenue, El Paso, TX 79968, USA.

³Border Biomedical Research Center, University of Texas at El Paso, 500 W University Avenue, El Paso, TX 79968, USA

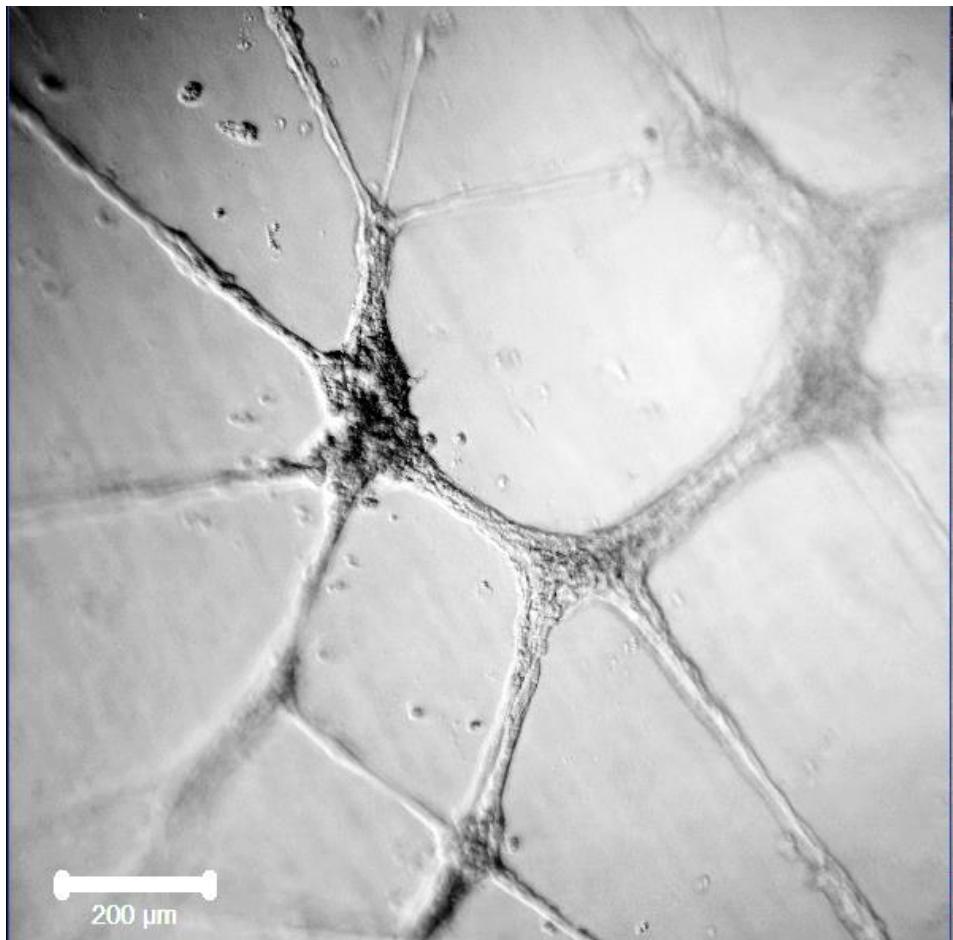
⁴Department of Biomedical Engineering, The University of Texas at Austin, 1 University Station, Austin, TX 78712, USA.

*Corresponding Author: bjoddar@utep.edu.

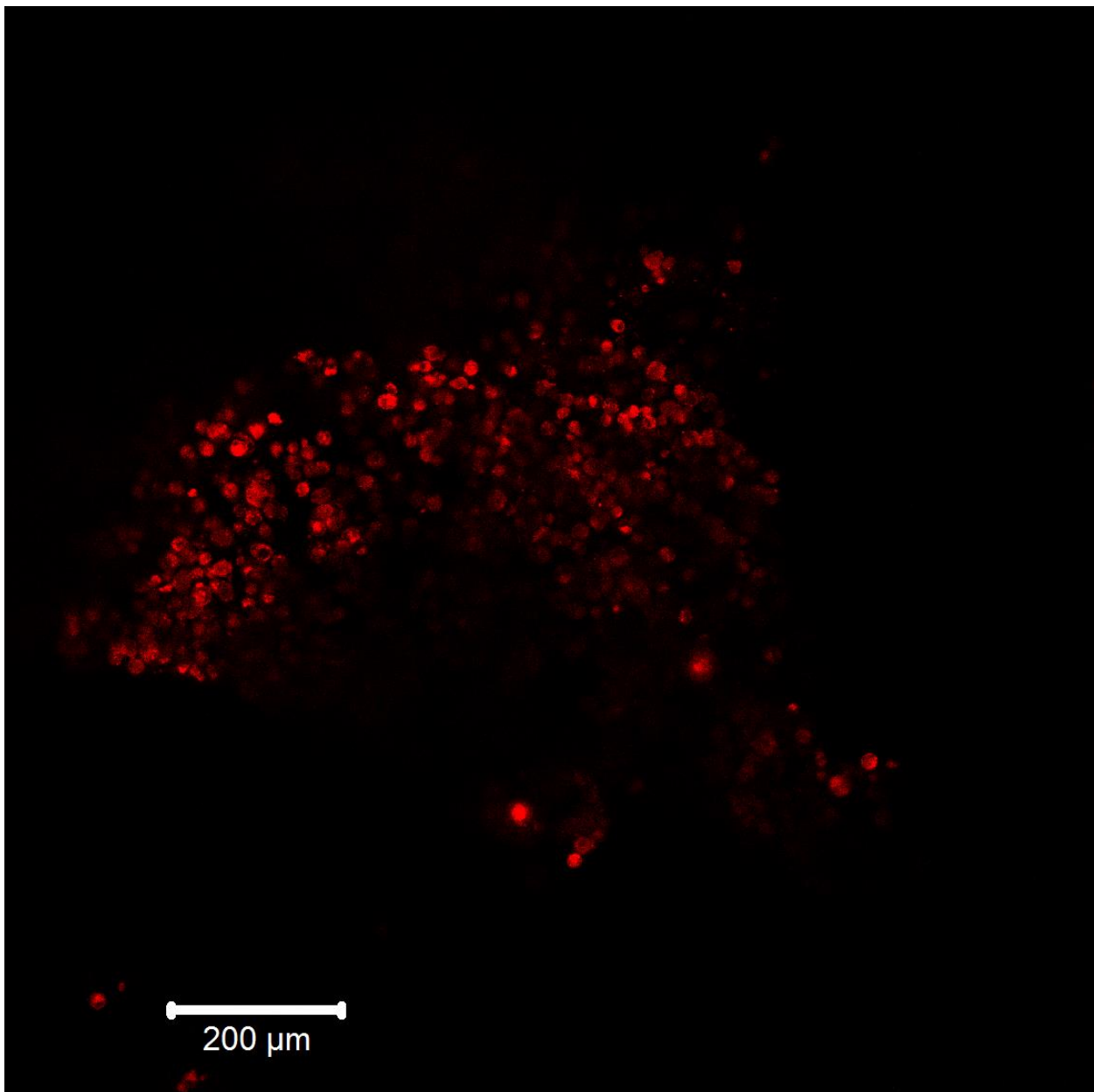
Optimization of Alginate Gels: Three different concentrations of MVG alginate gels (4, 7, and 10% w/v) were each crosslinked with three different calcium carbonate concentrations (10, 30, and 50 mg/mL). The resultant hydrogels were then tested for their elastic modulus and plotted as seen in **SF1**. A quadratic line was then fitted to each of the three-alginate gels on MATLAB and coefficients and a goodness of fit was produced. From these results, a “fibrotic” gel was chosen to be synthesized with 50 mg/mL of calcium carbonate and 10% (w/v) MVG alginate as it produced the stiffest hydrogel from all trials. Next, because “physiologic” stiffness’s in the heart are seen to be between 9-10 kPa, a value of 9.5 was used for the y-variable in the quadratic equation for the 7% alginate, and it’s appropriate coefficients were used to solve for the optimum amount of calcium carbonate needed to produce gels of that stiffness. The same procedure was done with the 4% alginate quadratic equation and coefficients to produce an “embryonic” gel with a stiffness from 1-3 kPa. The final calculated and optimized concentrations of calcium carbonate needed to produce the three hydrogels used in the main study are summarized in **Figure 1** of the main text. The values for GDL were then calculated by keeping the same ratio of CaCO₃ to GDL as described in other studies¹ and as outlined in the main text.



Supplementary Figure 1. Three concentrations of MVG alginate (4, 7, 10 % w/v) were each cross-linked with three different concentrations of calcium carbonate (10, 30, 50 mg/mL) and fitted with a quadratic equation in order to find optimum polymer and crosslinking concentrations that produce hydrogels with varying degrees of stiffness's, as reported in the manuscript.



Supplementary Figure 2. Cellular networks established by human AC16 cells when cultured atop 2D Matrigel coated wells. This confirms the networking behavior of these cells and facilitation by the Matrigel coating.



Supplementary Figure 3. Cellular networks are not formed when Matrigel is excluded from the gel confirming the role of Matrigel in network formation. Shown above are human AC16 CM cells pre-stained with PKH23 (red) and included within the gels made without addition of Matrigel after 120 hours of in vitro culture. However, the highest quantity of Ca^{2+} and GDL was used in this case (Stiff gels: Table 1) which confirms that these concentrations are not cytotoxic to cells.